First steps in the fine-tuning of the OTF-FSw method at Yebes-40m radiotelescope

David San Andrés de Pedro, María Jesús Jiménez Donaire

Informe Técnico IT-CDT 2022-02

Revision history

Version	Date	Author	Updates
1.0	04-02-2022	David San Andrés	First version
1.1	14-02-2022	Pablo de Vicente	First revision
1.2	05-03-2022	David San Andrés	Corrections and updates

Contents

1 Introduction

This technical report is the culmination of my work in the curricular undergraduate practices supervised by María Jesús Jiménez Donaire (astronomer at the National Astronomical Observatory - OAN by its acronym in spanish - in Madrid) that I developed during the months of February to May 2021 at the Yebes radio astronomical observatory, in the province of Guadalajara, Spain. The main objective was to actively contribute to the fine-tuning of the on-the-fly (OTF) *frequency-switching* observational method (hereafter OTF-FSw), one of the observational methods involving the OTF strategy, that has not yet been characterized and tested with the 40m radio telescope located in the above-mentioned observatory (hereafter Yebes-40m). However, due to a serious failure of the telescope that occurred in these months, these novel observations for Yebes-40m telescope were not available from the beginning of the practices, so we worked with observations already made using the same OTF strategy but with *position-switching* method (hereafter OTF-PSw), which has been successfully implemented in Yebes-40m. The main objective then turned to analyse in more detail the performance and implementation of the OTF-PSw method with Yebes-40m, previously done by my supervisor (see [1]), combined with a preliminary analysis of the OTF-FSw observations in contrast with those using OTF-PSw.

The OTF strategy, compared to classical pointing methods, allows to obtain very homogeneous maps (in terms of noise level) of large areas in the sky in a very efficient way, as the telescope moves smoothly and quickly over the region while data is continuously being collected. While in OTF-PSw method the telescope has to move from an OFF position (where the sky emission polluting the data from the source of interest will be measured) to an ON position held by the source of interest (actually, several ONs sharing the same OFF to cover the region); the OTF-FSw method cyclically changes the center frequency of the local oscillator without requiring OFF positions, being always ON so that the same spectrum is measured twice but shifted in frequencies and, by subtracting one from the other, a lower noise level is achieved. This makes it ideal for the case of narrow lines.

In order to improve these techniques in Yebes-40m, an observational proposal in DDT format was drafted (see appendix A) requesting new observations in OTF-FSw mode of the same region studied with OTF-PSw, but replacing the scanning pattern used in the latter with a *raster scanning pattern* instead. This was an attempt to correct those defects found in the OTF-PSw observations (see subsection 5.1).

This report is organised as follows: in section 2 we describe the radio observations performed and the properties of Yebes-40m telescope. In section 3 data processing and fundamental analysis tools used are detailed, presenting in section 4 the main results obtained. Finally, in section 5 we outline other problems found when performing OTF strategy with Yebes-40m telescope, summarising in section 6 the main conclusions of this technical report.

2   Observations

2.1   The Yebes-40m radiotelescope

The 40m telescope located in Yebes Observatory (Guadalajara, Spain) is one of the main radio astronomy facilities in Spain and it is operated by the National Geographic Institute (IGN by its acronym in spanish). This huge antenna follows a Nasmyth-Cassegrain structure, consisting of two reflectors: a parabolic primary reflector and a secondary hyperbolic one. It has an alt-azimuthal design, configured around a vertical and horizontal perpendicular rotation axis (called azimuth and elevation axis respectively). Rotation around the vertical axis varies the azimuth (compass bearing) of the pointing direction of the instrument, while rotation around the horizontal axis varies the altitude angle (elevation) of the pointing direction, from the horizon to the celestial zenith. The antenna is capable of rotating up to $3 \, \mathrm{degrees/second}$ and its tracking accuracy reaches 0.6 arcsec, 15 arcsec with wind peak velocities up to $10 \, \mathrm{m/s}$, when tracking becomes unreliable (see [2]).

This radio telescope is commonly used for single-dish observations and covers a frequency range from 2.2 GHz to approximately 90 GHz. It is regularly employed as part of interferometric observations for both geodesy and astronomy, being a key element of the European VLBI Network (EVN). However, despite the wide range of frequencies it covers, this report is focused on mapping the details of the OTF observations carried in the W band, between frequencies in the range $\sim 72 - 91$ GHz.

2.2   The observation region: The Integral-Shaped Filament

In this report, observational data of the same region using both OTF-PSw and OTF-FSw methods is analysed. This observation region corresponds to a part of what is known as *Orion's Integral-Shaped Filament*, an active star-forming region in the northern side of Orion A, one of the two giant molecular clouds that give shape to the Orion Molecular Cloud Complex and the most intense, active and best studied star-forming region in the local neighborhood of the Sun, hosting the birth of thousands of young stars and protostars [3, 4]. The whole filament is ~ 8 pc long, not being our objective to trace it in full. In fact, our region of interest is much smaller and defined as a rectangular mosaic (see figure 1) of two adjacent $100'' \times 100''$ maps. These two fields are centered on RA 5h35m14.2s, DEC $-5º22'21.5''$ and RA 5h35m14.2s, DEC $-5º22'41.5''$ (J2000) respectively.
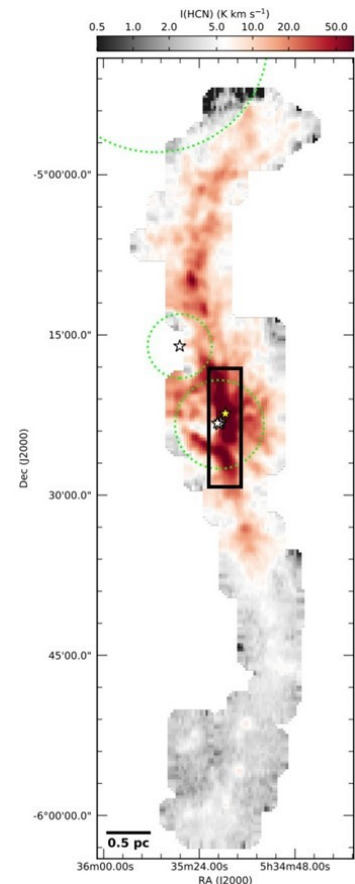
Figure 1: The *Integral-Shaped Filament* observed in HCN ($J = 1 \rightarrow 0$). The region inside the black rectangle is what will be mapped with Yebes-40m observations. Image adapted from [5].

2.3   Observations set-up

The two fields in which our observation region was divided were mapped independently in the horizontal and vertical directions with scans offset by $7''$ to ensure Nyquist sampling and using both OTF-PSw (already available) and OTF-FSw methods (new acquisition). For the former mapping mode, an emission-free reference OFF position close to Orion was used, which is not needed for the latter. In both observations, the telescope pointing and focus were checked every one to two hours through pseudo-continuum observations of Orion A.

Observations using OTF-PSw method were carried out at the Yebes-40m telescope on January 15-17, 2020 for a total exposure time of $\sim 5\mathrm{h}$ and using the W band with dual polarization. While using the W band allows to obtain an instantaneous bandwidth of 18.5 GHz per polarization, we exclusively employed two of the backends available, S7 and S8, which cover the frequency ranges $86.6 - 89.1$ GHz and $88.9 - 91.4$ GHz, respectively. The data were processed using the Fast Fourier Transform spectrometers (FFTs), with a spectral resolution of 38 kHz (the highest available) due to the large width of some lines that fall on this range such as in the case of HNC ($J = 0 \rightarrow 1$). An schematic of the scanning pattern used is shown in figure 2a.

On the other hand, observations using OTF-FSw method were carried out at the Yebes-40m telescope on May 28, 2021 for a total exposure time of $\sim 2\mathrm{h}$ and using the same instrumental configuration: W band with dual polarization and backends S7 and S8. An schematic of the scanning pattern used in this case is shown in figure 2b.

(a) OTF-PSw scanning pattern   (b) OTF-FSw scanning pattern
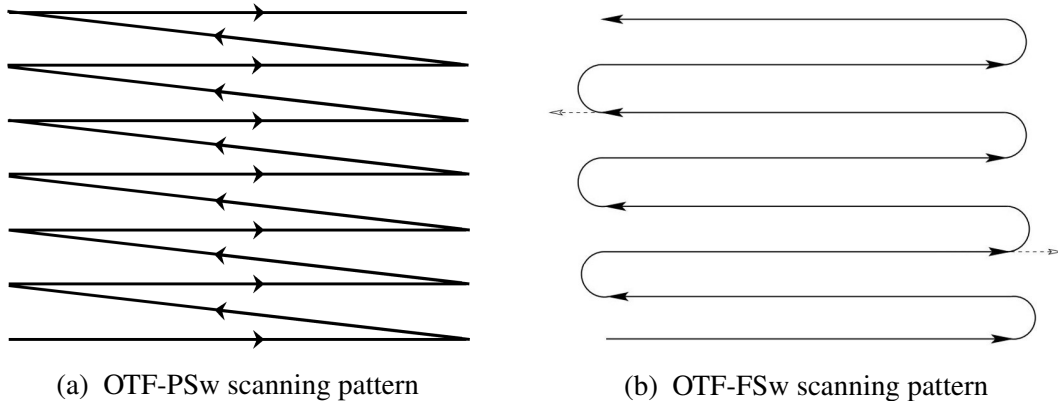
Figure 2:   Scanning patterns used with Yebes-40m for covering the whole region with both methods. Arrows indicate the direction followed by the antenna while scanning, but data is collected only when moving horizontally in both methods.

3   Methodology

With previous data available for this region using the OTF-PSw technique, we have extracted maps of it to characterise the distribution of main dense gas tracers (among other molecules) such as HCN, HNC and HCO$^+$, typically found in the interstellar medium. We also constructed the central spectra for each of these lines and the associated 0th moments (integrated intensity), helping to trace the star formation. This is because allow to study the distribution of dense and

cold gas from which we expect stars to form or to have formed. With regard to the recently obtained OTF-FSw data, we have only constructed the central spectra for the same lines studied using OTF-PSw data in order to make a brief comparison with those generated with the latter method.

In this section we will describe all the steps followed to obtain the results presented in the next section, starting with the correct processing of the raw data as it comes directly from the telescope.

3.1   Initial data processing

The data produced by the telescope are delivered in FITS format ([6]) and CLASS format. We have used the latter for a further processing of the spectra. For this task we have used the CLASS program within the GILDAS software ([7]), oriented to data processing in the (sub-)millimetre band of the spectrum.

The next step consists in building individual cubes for each emission line studied but separately (see subsection 3.2 to see the lines selected), locating them in the appropiate *backend* section. Once all the observations collected in that *backend* section have been selected, we take the first one corresponding to a spectrum of a point in the plane (RA, DEC) tracing the studied region, for which a measurement was made. To find the line of interest it is as simple as positioning the 0 of velocities at its rest frequency and opening a frequency window that includes the line and part of the spectrum outside at both sides of the line. However, all lines show a shift of nearly 9 km/s, which makes the rest frequency align with that velocity and not 0 (this will be the v_{LSR}, inherent to the source itself). Then, a baseline should be applied to correct the spectrum so that the continuum corresponds to zero intensity. This process is then repeated for each point in the (RA, DEC) plane, saving everything in a cube for each line.

As seen, it is necessary to know the rest frequency for each line, using for this purpose any of the available astronomical spectral line catalogues, such as *Splatalogue*.

3.2   Selected emission lines

Being the main purpose of this report to analyse the efficiency and performance of OTF-PSw and OTF-FSw methods at Yebes-40m, we do not seek a priori to study the emission of any specific molecule. Indeed, it would be more appropriate to analyse emission lines corresponding to different molecules to extract as much information as possible. For this reason, we have selected the intense lines of HNC ($J = 1 \rightarrow 0$) and HCO$^+$ ($J = 1 \rightarrow 0$), the also very intense transition HCN ($J = 1 \rightarrow 0$) that exhibits a more complicated structure (hyperfine splitting), the weaker lines of H^{13}CO$^+$ ($J = 0 \rightarrow 1$) and C$_2$H ($J = 3/2 \rightarrow 1/2$) that will show differences in the S/N achieved with both methods, along with the very broad line of SiO ($J = 2 \rightarrow 1$). All these lines and their parameters are summarized in table 1.

Despite the large width of some lines such as in the case of HCN ($J = 1 \rightarrow 0$) or SiO ($J = 2 \rightarrow 1$), they will still be observable with OTF-FSw method without being auto-contaminated, as they do not overlap with any nearby line.

Molecule	Transition(s)	Rest frequency (MHz)	*Backend*	Scientific use
$H^{13}CO^+$	$J = 1 \to 0$	86754.288	S7	HCO^+ isotope, tracing the same as the main isotopologue but being less abundant
SiO	$J = 2 \to 1$	86846.960	S7	Characterises the presence of jets and shocks, indicating high velocities for the gas
C_2H	$J = \frac{3}{2} \to \frac{1}{2}$	87316.925	S7	Photo-Dissociation Regions (PDRs) tracer (regions highly exposed to external radiation and therefore hotter)
HCN	$J = 1 \to 0, F = 1 \to 1$	88630.416	S7	Cold and dense gas tracer
	$J = 1 \to 0, F = 2 \to 1$	88631.847		
	$J = 1 \to 0, F = 0 \to 1$	88633.936		
HCO^+	$J = 1 \to 0$	89188.525	S8	Medium-dense but highly abundant gas tracer, specially in low extinction regions
HNC	$J = 1 \to 0$	90663.568	S8	Cold and dense gas tracer

Table 1: Lines selected for our study sorted by increasing frequency. The last column shows briefly why it would be useful to study this line in a scientific context. All transitions correspond to $\nu = 0$, being ν the vibrational quantum number, while J and F are those quantum numbers associated with rotational and hyperfine structure levels respectively.

3.3 Central spectra, 0th moments and channel maps

Once individual cubes have been constructed for each of the lines (species) of interest, information about the distribution of those molecular species can be found by constructing different maps and spectra.

Fist of all, these cubes can be quickly visualised by making use of a channel map, that allow to see at a glance the emission (for the whole region covered) of a specific line by splitting it into the frequencies defining the entire line and crafting an emission map for each one of these frequencies.

Another interesting map that can be constructed is what is known as a *0th moment map* (M_0), which captures the integrated intensity of the source being mapped (in short, it would deliver a single map by combining all the emission shown in channel maps). It is also useful to compute the *1st moment map* (M_1), which outlines the gas velocity field, but in this report this is not shown. The expressions for both moments already mentioned are:

$$M_0 \text{ [Kkm/s]} = \int I_v dv \qquad ; \qquad M_1 \text{ [km/s]} = \frac{\int v I_v dv}{M_0}$$

where v is the gas velocity and I_v the intensity. In radio astronomy, intensity is usually measured in Kelvin (K) since what is typically measured is what is known as the antenna temperature (Ta*), defined as the temperature of the blackbody that would give the same power as that received by the source (similar to the brightness temperature T_B in the Rayleigh-Jeans approximation). The x-axis in the spectra is usually expressed in velocities rather than frequencies, being in fact more convenient.

Finally, to compare both observational methods, central spectra were constructed for each line of interest. These correspond to the combination of all spectra collected between the central position of the map and an offset from that position of ±10 arcseconds in RA and DEC, being the region covered by the telescope's main beam when doing a single pointing shot. On one hand, a gaussian fit was made to determine the total intensity of the lines and their FWHM. On the other hand, the noise level was evaluated from the rms value of that part of the spectrum without line emission, finding it to be quite homogeneous throughout the map (typical of observations following the OTF strategy).

4   Results

4.1   Channel maps for OTF-PSw observations

In this first section, we present the channel maps associated with the emission lines HCN ($J = 1 \rightarrow 0$) and HNC ($J = 1 \rightarrow 0$) along with the whole region mapped, by separating this emission as a function of frequency for those close to the rest frequency. It can be seen how the contour levels become larger (show a more extended emission) as we approach frequencies closer to the rest frequency of each line. These maps are only generated by using OTF-PSw observations.
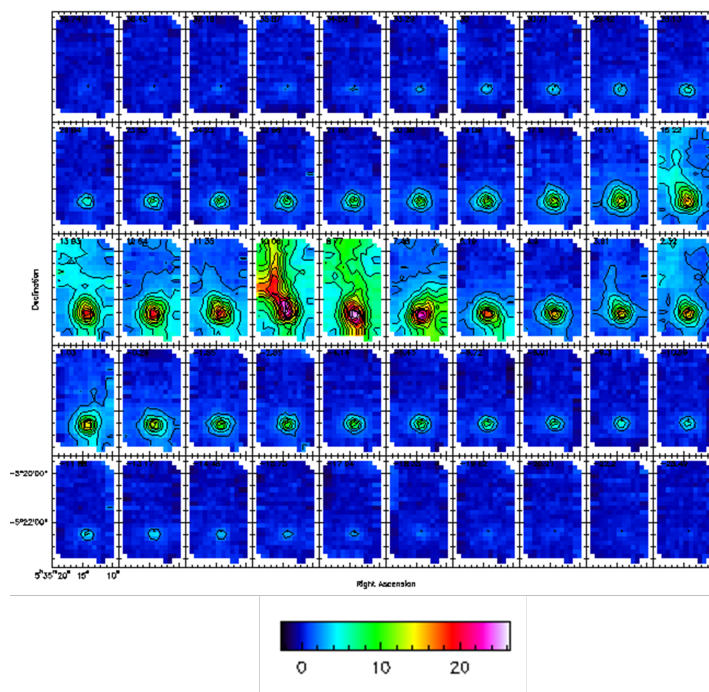
Figure 3: Channel map for HCN ($J = 1 \rightarrow 0$). The offset frequency from map to map is about 0.6 MHz (about 2.4 km/s in velocities), while the contour lines represent a separation of 2 K in intensity.
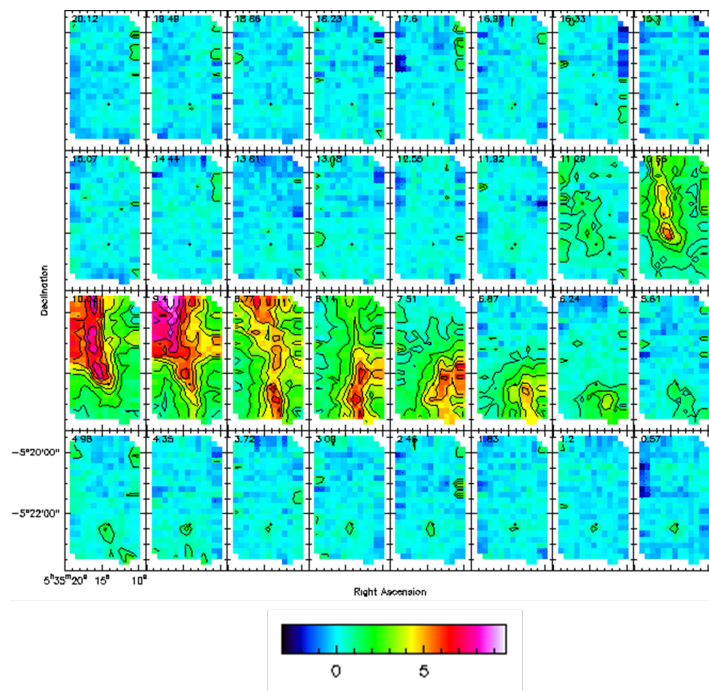
Figure 4: Channel map for HNC ($J = 1 \rightarrow 0$). The offset frequency from map to map is about 0.7 MHz (about 2.2 km/s in velocities), while the contour lines represent a separation of 1 K in intensity.

4.2 0th moments for OTF-PSw observations

Having shown in the previous section the channel maps constructed for HCN and HNC, the next natural step is to obtain the 0th moment maps for all the species studied. However, two of them (C_2H and $H^{13}CO^+$) are not displayed as they do not contain relevant information and do not show anything clear. These maps are only generated using OTF-PSw observations.
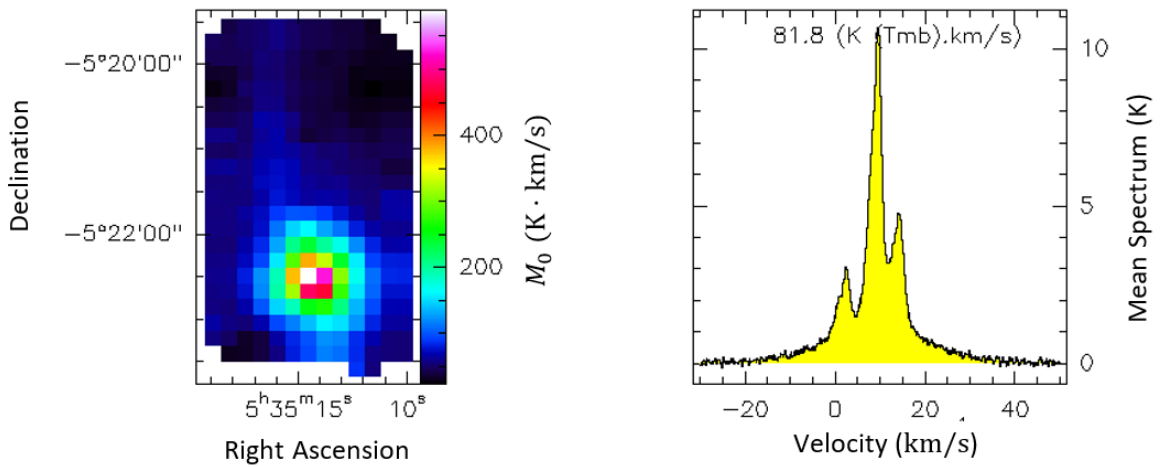
Figure 5: 0th moment for HCN ($J = 1 \rightarrow 0$) using OTF-PSw. *Left*: 0th moment map for this molecule. It can be noticed the presence of an active star-forming region (highest integrated emission) on the bottom. The pixels on the right-hand side of the map show a strange behaviour probably caused by the way the telescope performs the sweep when covering the region. *Right*: average spectrum for the whole map, enclosing a total area of 81.8 Kkm/s.
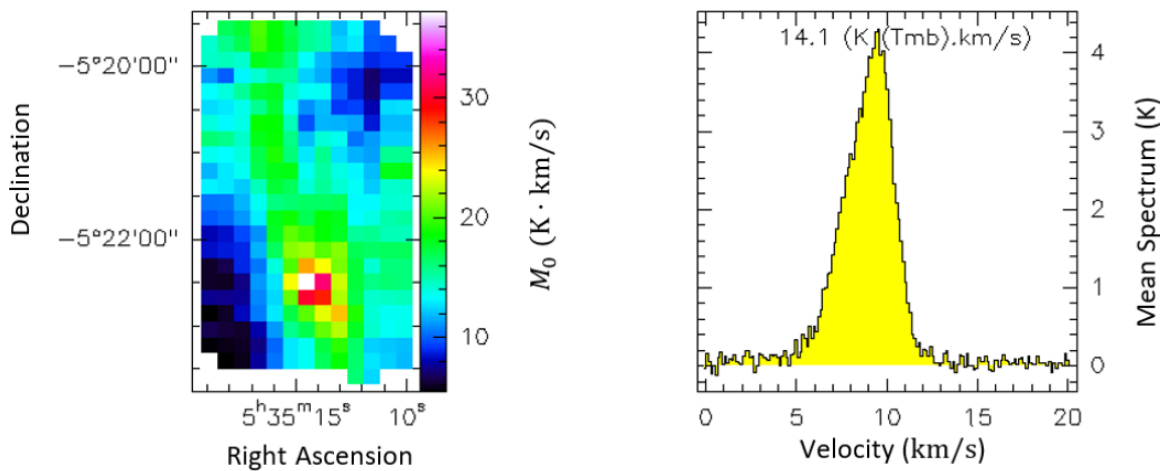
Figure 6: 0th moment for HNC ($J = 1 \rightarrow 0$) using OTF-PSw. *Left*: 0th moment map for this molecule. It can be also noticed the presence of an active star-forming region on the bottom. It continues being noticeable the strange behaviour of the pixels on the right-hand side of the map. *Right*: average spectrum for the whole map, enclosing a total area of 14.1 Kkm/s.
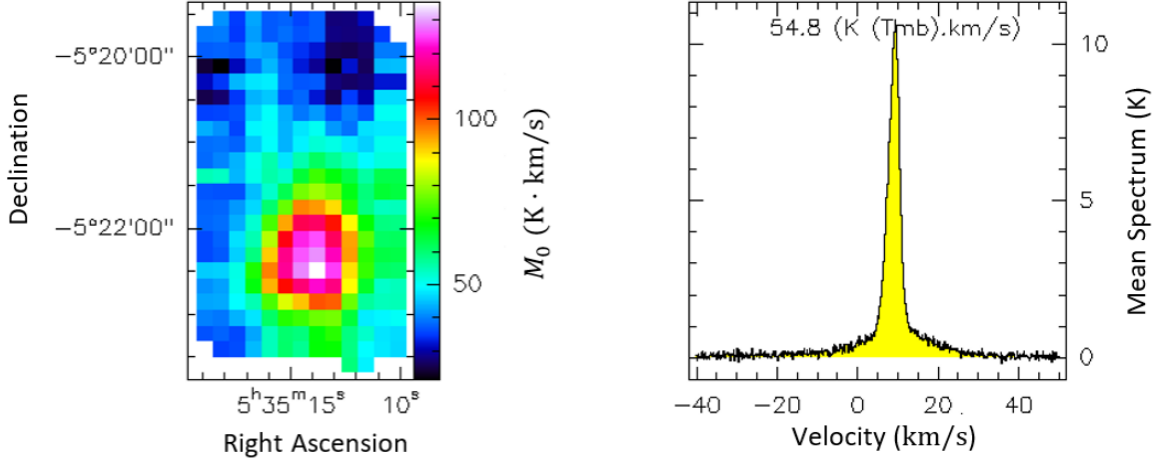
Figure 7: 0th moment for HCO$^+$ ($J = 1 \to 0$) using OTF-PSw. *Left*: 0th moment map for this molecule. It can be also noticed the presence of an active star-forming region on the bottom. The pixels on the right-hand side of the map continue showing a strange behaviour. *Right*: average spectrum for the whole map, enclosing a total area of 54.8 Kkm/s.
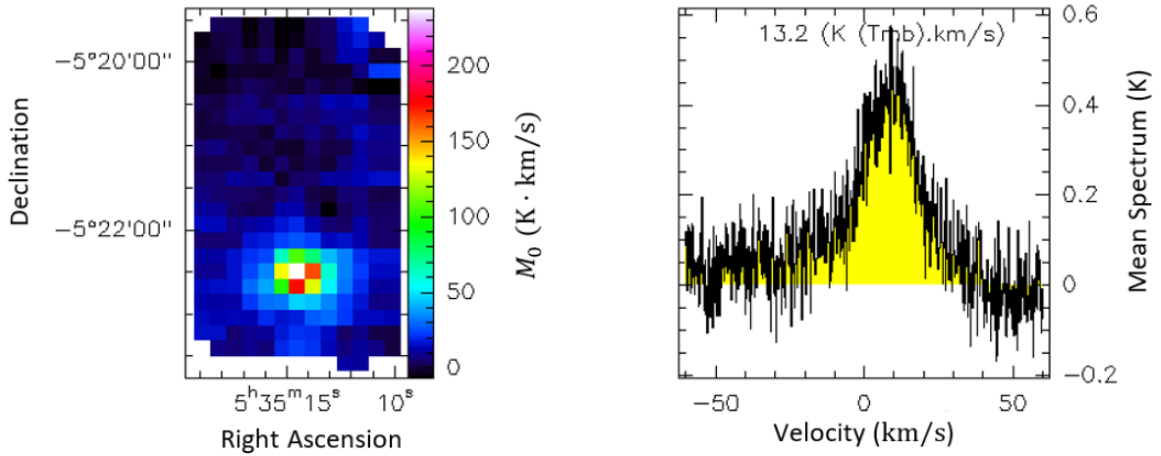
Figure 8: 0th moment for SiO ($J = 2 \to 1$) using OTF-PSw. *Left*: 0th moment map for this molecule. It can be also noticed the presence of an active star-forming region on the bottom. The strange behaviour of the pixels on the right-hand side of the map continue appearing. *Right*: average spectrum for the whole map, enclosing a total area of 13.2 Kkm/s, being the noisiest among those shown.

All maps displayed in figures 5-8 reveal the presence of an active star-forming region at the bottom of the region observed, reflected in a higher emission compared to the rest of the map. It is also noticeable than an extended emission, seen in HCN and HNC maps, takes the shape of a tail in the upper part of both maps, probably indicating the presence gas. As seen, all the maps also show a strange behaviour of the pixels found on the right-hand side of the map (as the two pixels involved show exactly the same intensity value), probably due to those inaccuracies found in telescope pointing while scanning. This will be discussed in more detail in section 5.1. All these maps are consistent with what is shown in [1, 5].

4.3 Central spectra: comparison between OTF-PSw and OTF-FSw

With the aim of comparing both observational methods already presented, central spectra for all selected transitions have been constructed (see table 1). These spectra are shown in figures 9-14 and it can be seen how there are subtle differences between those extracted with one method and the other, although the shape and width of the lines scarcerly varies. For each of the studied lines, a gaussian fit has been made in order to extract the width of the lines to be compared. However, in most cases this will not reproduce the whole emission, being necessary to introduce other components. When using a gaussian fit to the intensity of the line, the following expression is applied:

$$I(v) = \frac{A}{\sqrt{2\pi\sigma^2}} \exp\left(-\frac{(v-v_0)^2}{2\sigma^2}\right)$$

where $I(v)$ represents the line intensity as a function of velocity v, A is the area beneath the curve (measured in units of Kkm/s), σ is the standard deviation and v_0 the peak velocity. This expression is used after applying a baseline.

To determine the width we use instead the FWHM parameter, which represents the width of the line at which the intensity is half the peak emission and is connected with the standard deviation through the expression $\mathrm{FWHM} = 2\sqrt{2\log 2}\sigma$. In the case of HCN ($J = 1 \to 0$) line, a fit using four components was made: three characterising the peaks and another tracing the emission itself.

The most remarkable thing is that the intensity scale differs significantly when using OTF-PSw and OTF-FSw methods for mostly every line. This may be related to a different telescope gain between both sets of measurements. The OTF-FSW and the OTF-PSW were done in different seasons (year and five-month difference between one observation and another) and therefore different conditions. We lack a common flux calibrator in both epochs, which would have allowed to check calibration differences. For this reason, the comparison of central spectra for both methods will be focused only attending to the shape and width of the observed emission lines.

Finally, C_2H and $H^{13}CO^+$ weak lines reveal that a higher S/N ratio is achieved with OTF-FSw observations compared with those using OTF-PSw data, although having similar integration times. However, this trend will only be confirmed when studying quite a few more weak lines, which is not our case, so no clear conclusion can be drawn.
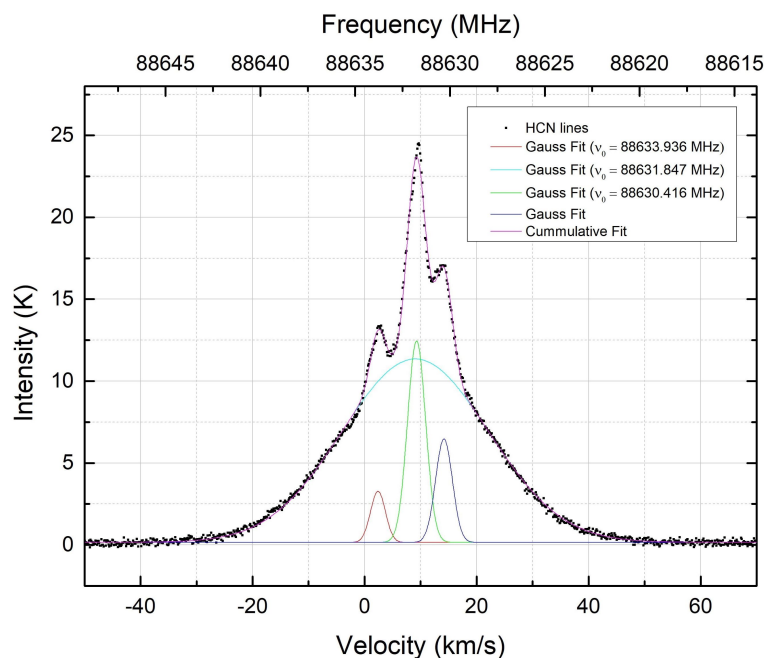
(a) HCN ($J = 1 \rightarrow 0$) central spectrum with OTF-PSw.
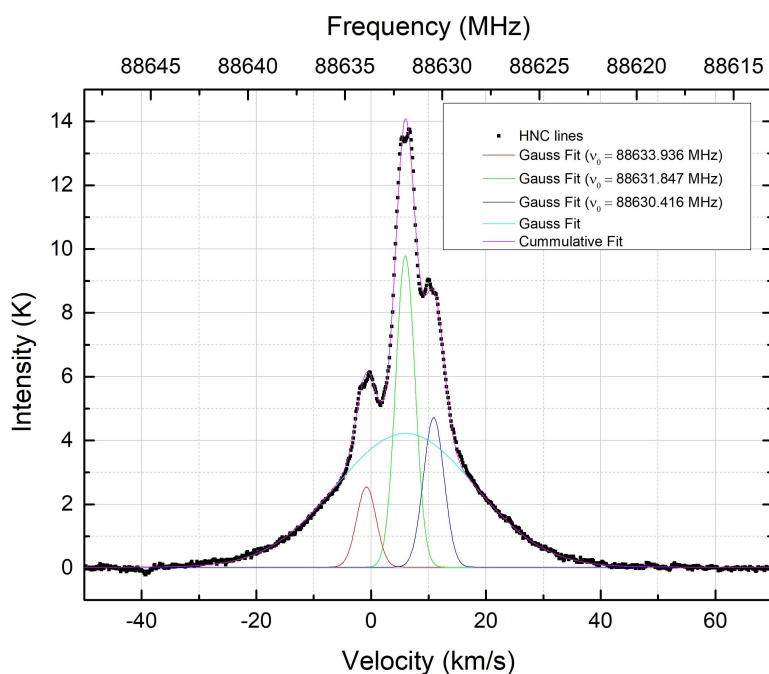
(b) HCN ($J = 1 \rightarrow 0$) central spectrum with OTF-FSw.

Figure 9. HCN ($J = 1 \rightarrow 0$) central spectrum with OTF-PSw (upper panel) and OTF-FSw (lower panel). The whole emission of the line is splitted into three separate peaks (components) with a similar central frequency due to the hyperfine structure. FWHM values for these three components (sorted from lowest to highest frequency) are 3.53(6), 3.81(3) and 3.13(9) for OTF-PSw, while 4.23(6), 3.95(5) and 4.02(8) km/s for OTF-FSw.
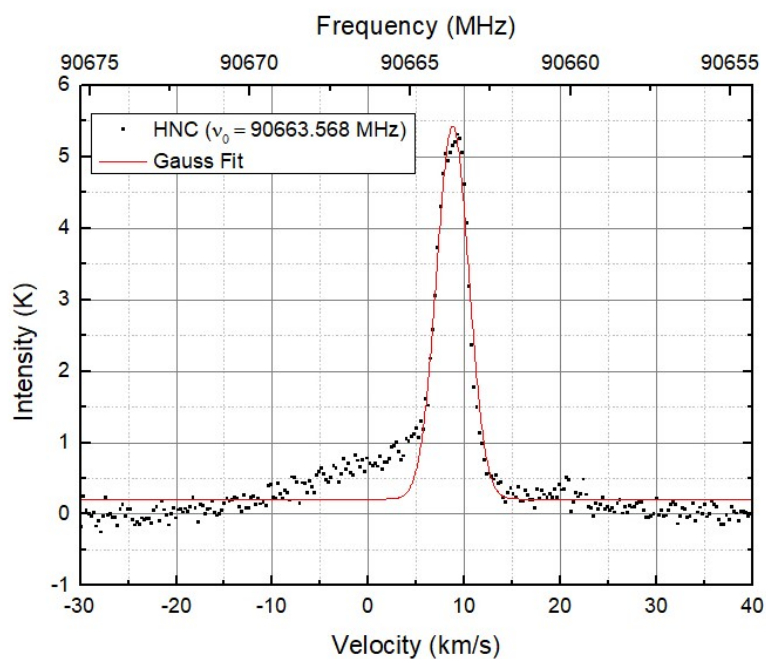
(a) HNC $(J = 1 \rightarrow 0)$ central spectrum with OTF-PSw.
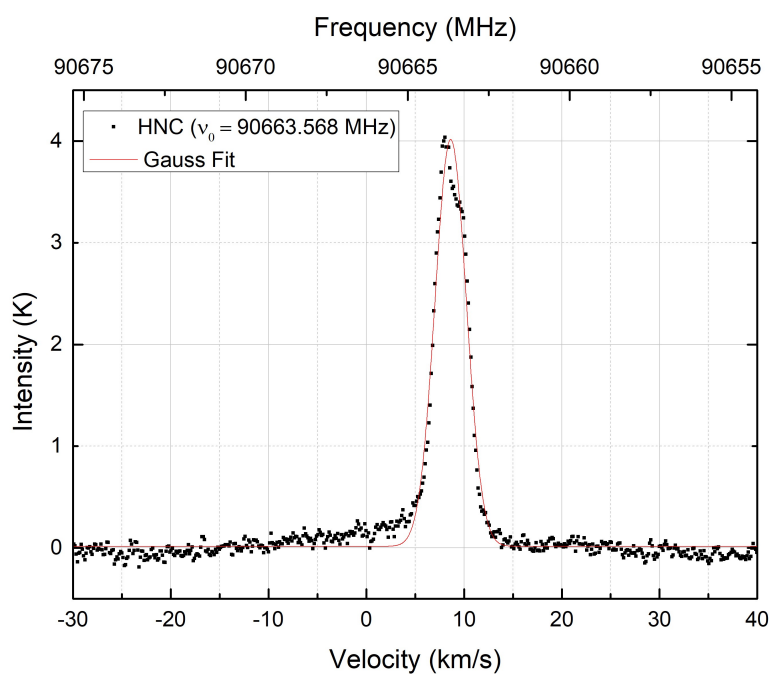
(b) HNC $(J = 1 \rightarrow 0)$ central spectrum with OTF-FSw.

Figure 10. HNC $(J = 1 \rightarrow 0)$ central spectrum with OTF-PSw (upper panel) and OTF-FSw (lower panel). Both lines show a similar profile, although the spectrum computed for OTF-PSw shows a more profound asymmetric emission on the left side of the line than OTF-FSw spectrum. FWHM values are 3.94(9) km/s for OTF-PSw and 3.76(3) km/s for OTF-FSw, being quite similar.
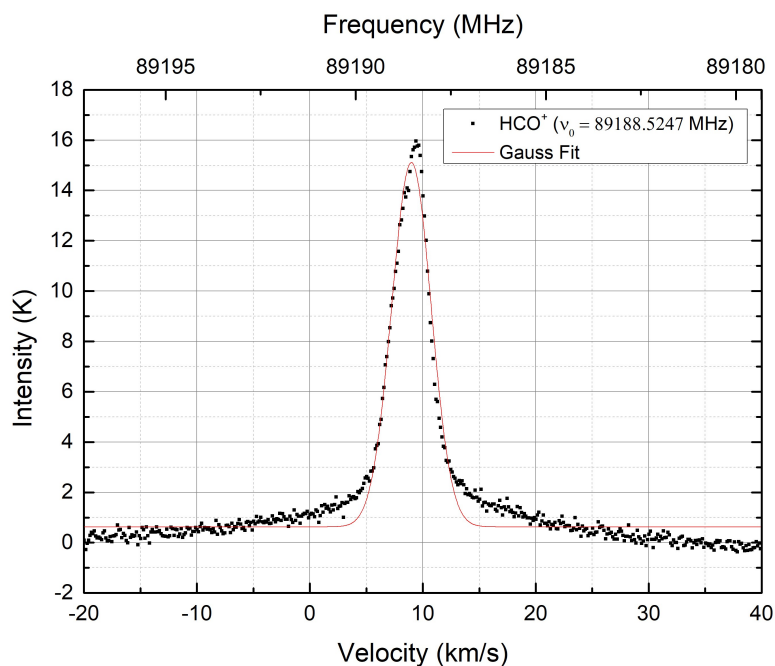
(a) HCO^+ $(J = 1 \rightarrow 0)$ central spectrum with OTF-PSw.
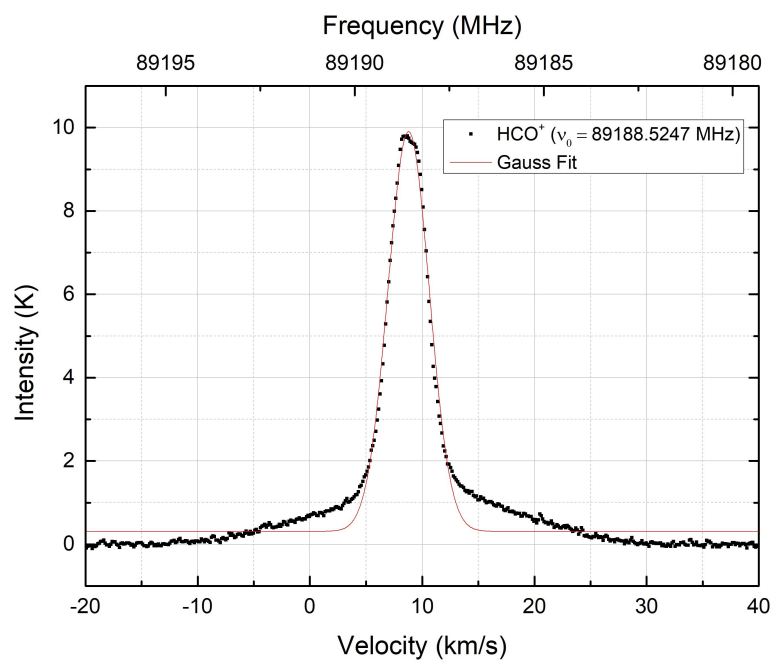
(b) HCO^+ $(J = 1 \rightarrow 0)$ central spectrum with OTF-FSw.

Figure 11. HCO^+ $(J = 1 \rightarrow 0)$ central spectrum with OTF-PSw (upper panel) and OTF-FSw (lower panel). Both lines show a similar profile, revealing how a gaussian profiles itself does not reproduce the entire emission properly (because of the large tails). FWHM values are 4.11(5) km/s for OTF-PSw and 4.33(5) km/s for OTF-FSw, being very similar.
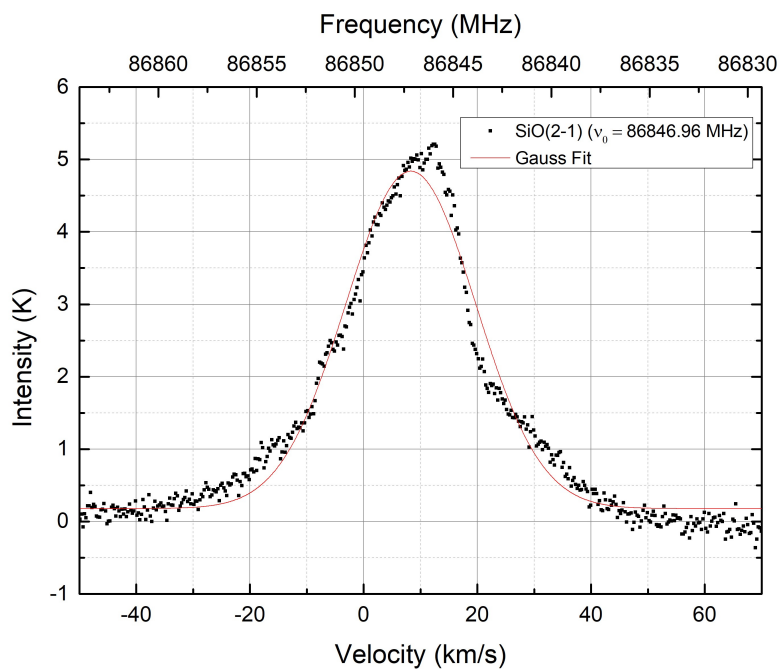
(a) SiO ($J = 2 \to 1$) central spectrum with OTF-PSw.
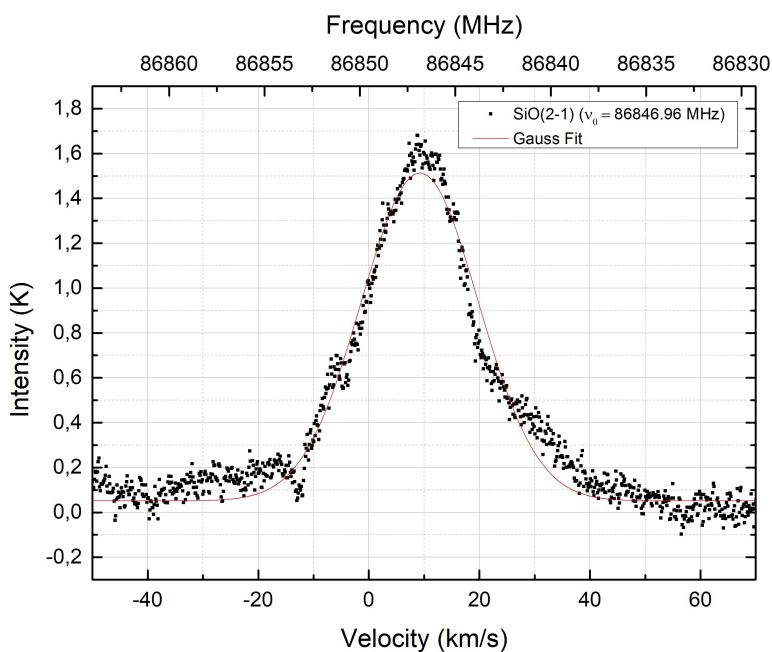
(b) SiO ($J = 2 \to 1$) central spectrum with OTF-FSw.

Figure 12. SiO ($J = 2 \to 1$) central spectrum with OTF-PSw (upper panel) and OTF-FSw (lower panel). Both lines show a similar profile and, in comparison with other spectra shown, they are noisier. FWHM values are 26.9(3) km/s for OTF-PSw and 25.0(2) km/s for OTF-FSw. It is one of the widest lines observed and this translates into greater differences when using both methods.
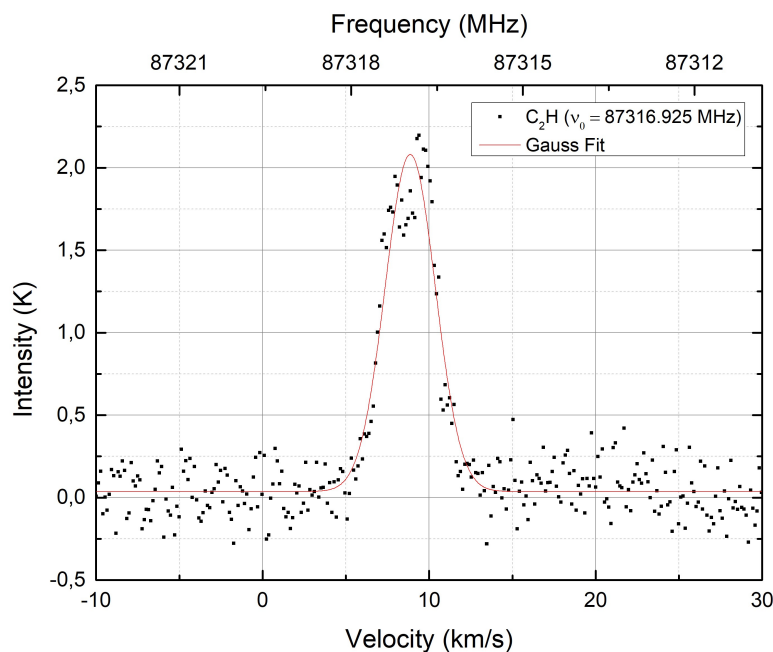
(a) C_2H $(J = \frac{3}{2} \to \frac{1}{2})$ central spectrum with OTF-PSw.
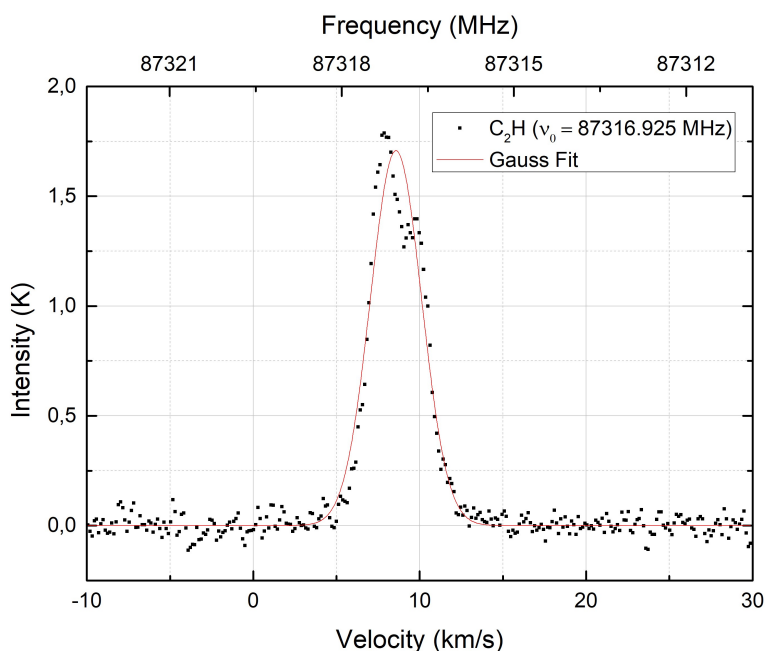
(b) C_2H $(J = \frac{3}{2} \to \frac{1}{2})$ central spectrum with OTF-FSw.

Figure 13. C_2H $(J = \frac{3}{2} \to \frac{1}{2})$ central spectrum with OTF-PSw (upper panel) and OTF-FSw (lower panel). Both lines present a similar profile and peak intensity. FWHM values are 3.55(9) km/s for OTF-PSw and 3.62(6) km/s for OTF-FSw, being very similar. It can be noticed that the noise level is higher for OTF-PSw than OTF-FSw, which may indicate that a higher S/N ratio has been achieved with the latter method for similar exposure time.
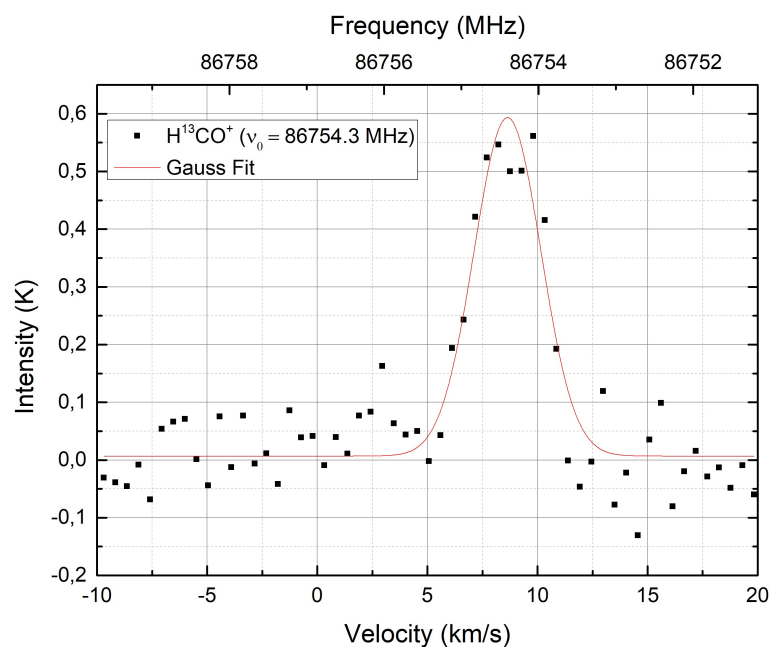
(a) $H^{13}CO^+$ $(J = 1 \rightarrow 0)$ central spectrum with OTF-PSw.
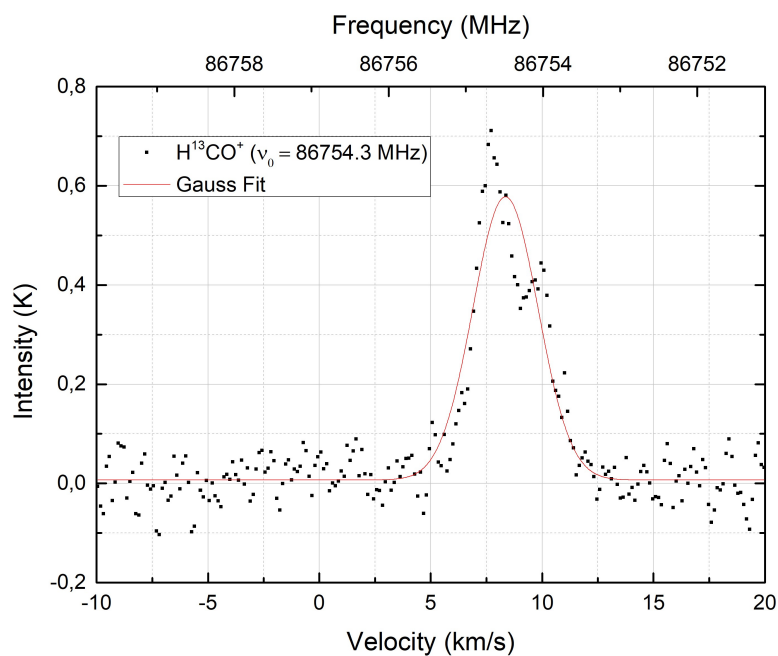
(b) $H^{13}CO^+$ $(J = 1 \rightarrow 0)$ central spectrum with OTF-FSw.

Figure 14. $H^{13}CO^+$ $(J = 1 \rightarrow 0)$ central spectrum with OTF-PSw (upper panel) and OTF-FSw (lower panel). The emission shown using OTF-PSw method is more buried in the noise and does not appear as a clear detection, unlike OTF-FSw, which reinforces the idea of having achieved a higher S/N ratio. Furthermore, the shape of the line is quite different when comparing both methods. However, FWHM values that are 3.57(0.26) km/s for OTF-PSw and 3.45(0.11) km/s for OTF-FSw, are closed.

4.4 RMS values for OTF-PSw and OTF-FSw spectra

Finally, to conclude our analysis comparing both observational methods, we have evaluated the rms value for each of the lines studied, which is taken by analysing the continuum around the line being studied and hence the noise level of the spectra. Figure 15 shows the ratio of the rms value of the OTF-PSw and OTF-FSw spectra for each emission line. It can be clearly seen how OTF-FSw observational method spectra exhibit lower rms values than OTF-PSw method ones, being the rms value with OTF-PSw at the very least twice the rms value archieved with OTF-FSw method, despite having similar integration times.
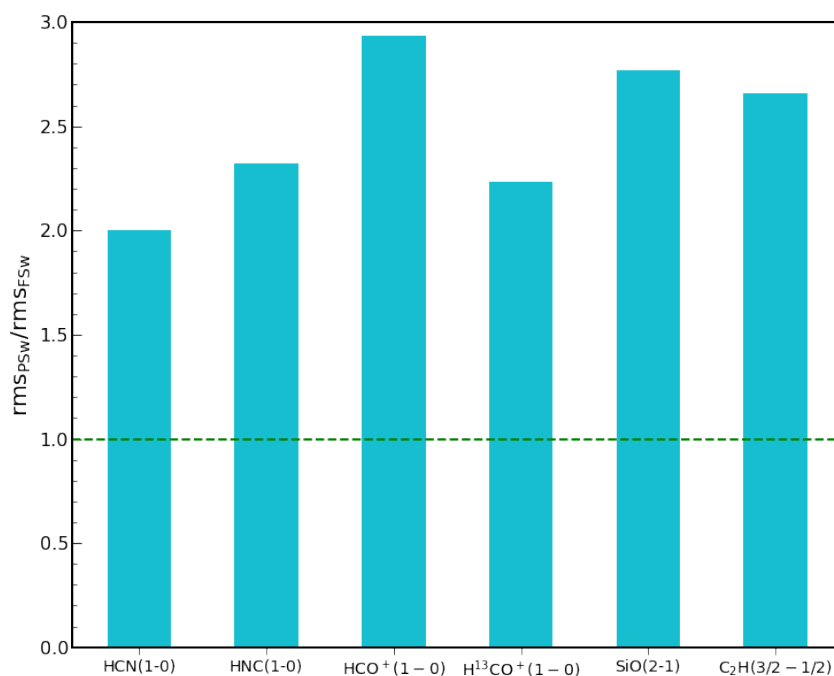
Figure 15. RMS values ratio taken from OTF-PSw and OTF-FSw spectra respectively, for each of the emission lines here studied.

5   Remarks and recommendations

The On-The-Fly method is an efficient and widely adopted observing technique used to map regions of the sky by slowly moving the telescope antenna, while data is continuously being taken in short time intervals. This technique differs from the traditional mapping strategies (also known as "step-and-integrate" or "ON-OFF" mapping) which consist of discrete integrations on the sky, and it is more effective when wide areas need to be surveyed in relatively short integrations. Observations performed in OTF mode are endowed with several advantages over usual position-switching observations.This technique significantly reduces observing overheads and also allows to cover the desired areas very rapidly, minimizing the effects of system variations and atmospheric changes, showing greater overall efficiency. However the base lines of the spectra are usually much less flat.

When comparing OTF-PSw and OTF-FSw methods, clear differences arise. For the former method an OFF position without emission of any kind should be used and in some cases this may imply moving the telescope far away from the source to be mapped. This might also be affected by atmospheric variations that translate into bad baselines and also the need for higher exposure times. In contrast, the latter method requires less exposure time because the telescope is always on the source. However, sky emission is not subtracted and sky emission lines continue appearing in the spectra (polluting other lines of interest). This method is also limited to the characterisation of narrow lines, as this method hides some areas of the spectrum where the folding remnant lies. This is specially important in chemically rich regions, where lots of emission lines will be found.

Following [1] analysis, there are two major modifications that can be implemented at the Yebes-40m telescope to make OTF (more specifically OTF-PSw) observations more efficient: reducing the time spent in OFF position, and changing the scanning pattern to a raster pattern instead. The latter has been done with newly obtained OTF-FSw observations, but other problems are identified. In the following section we describe all them.

5.1   Scanning patterns with Yebes-40m

As a final approach to contribute to the correct implementation of OTF-PSw and OTF-FSw methods in Yebes-40m, real scanning patterns followed by the telescope while taking data are depicted in figures 16a and 16b. They reveal important information on how the antenna moves to cover the whole region and what can be done to correct those shortcomings that appear.

Figure 16a shows the *z scanning pattern* chosen to perform OTF-PSw observations. Measurements are only taken during horizontal scans where data is gathered every 9 arcsec. For each horizontal scan, 11 data points (ONs) are collected and the telescope is then shifted to the OFF position. The time spent per ON position is 5.5 seconds, while in OFF position measurements take 28 seconds. By looking at the right-hand side, a small misalignment can be observed when the telescope is about to start a new horizontal scan. As [1] stated, the vertically drifted pattern we see at the initial point in every horizontal scan when the antenna positioned itself, is something that should be corrected. However, looking at the map as a whole, a nearly uniform picture is obtained.

(a) Real scanning pattern for OTF-PSw

(b) Real scanning pattern for OTF-FSw
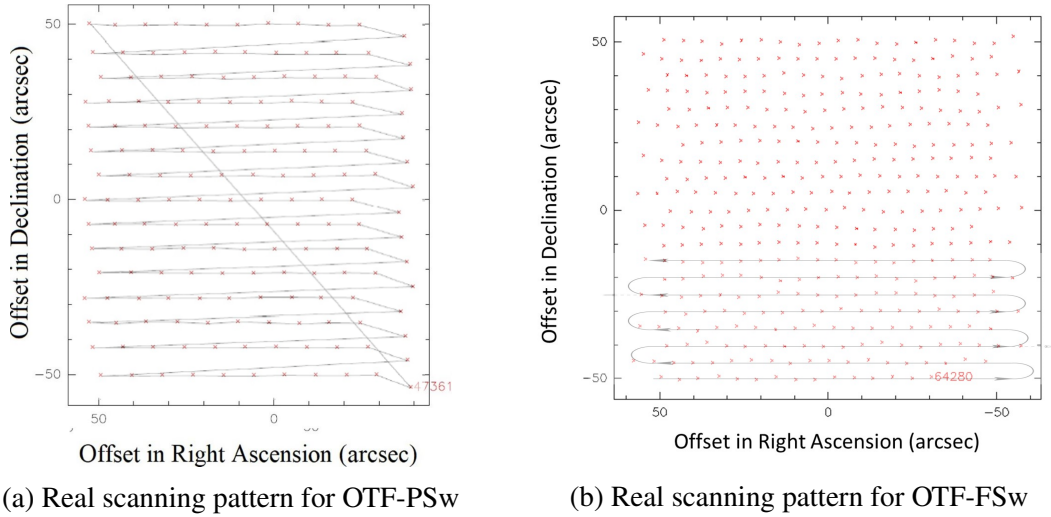
Figure 16. Real scanning patterns drawn by Yebes-40m when performing the observations with both methods (red blades). The schema presented in figures 2a and 2b is superimposed in black.

On the other side, figure 16b shows the *raster scanning pattern* implemented for OTF-FSw observations. Measurements are, as well, only taken during horizontal scans where data is collected every ~ 5.2 arcsec, having a total of 19 data points (ONs) per horizontal scan. As it can be seen in this figure, the region covered is slightly larger than 100 arcsec in RA direction. Seeing the map as a whole, Yebes-40m does not reproduce a perfectly homogeneous pattern as it can be observed due to a lack of alignment in the vertical direction.

Both figures indicate that further effort has to be made in order to achieve the highest efficiency possible when using these mapping techniques.

6 Conclusions

OTF-PSw and OTF-FSw implementation in Yebes-40m will help this telescope to continue on its journey to become a reference telescope for Spanish and worldwide astronomy by achieving the highest efficiencies result of a perfect implementation.

One of the current major problems regarding both methods rely on the way the antenna covers the region to be mapped, showing clear deviations from homogeneity both in horizontal and vertical coverage. Time spent on OFF positions should be also decreased to reduce observing overheads.

When comparing central spectra constructed for both methods, an apparently greater S/N was achieved with OTF-FSw observations when weak lines where studied, despite having similar integration times. This trend will be confirmed if more observations and deeper analysis are carried out. Nevertheless, the most important difference between both methods is that the intensity of mostly every line is much lower for OTF-FSw observations than OTF-PSw ones. Further observations with a common calibrator should be performed to find out if this is due to a calibration issue.

References

[1] Jiménez Donaire, M.J. On-the-fly observations of star forming regions with the Yebes-40m radiotelescope. OAN Technical Report 2020-05.

[2] de Vicente, P., Visus, M. Tracking errors at the 40 m radiotelescope. OAN Technical Report 2013-13.

[3] Bally, J. Overview of the Orion Complex. Handbook of Star Forming Regions Vol. I, ASP Conference Series, 2008.

[4] Johnstone, D., Bally, J. JCMT/SCUBA submillimiter wavelength imaging of the integral-shaped filament in Orion. The Astrophysical Journal, 510: L49–L53, 1999.

[5] Hacar A., Bosman A. D., van Dishoeck E. F. HCN-to-HNC intensity ratio: a new chemical thermometer for the molecular ISM, 2020, AA, 635, A4.

[6] MBFITS software, https://www.mpifr-bonn.mpg.de/4492985/mbfits

[7] GILDAS software, https://www.iram.fr/IRAMFR/GILDAS

A   DDT proposal for OTF-FSw observations

Testing the FSw-OTF observing mode with Yebes-40m radiotelescope

P.I.: David San Andrés de Pedro

The goal of this DDT proposal is to test and characterize the on-the-fly (OTF) technique using the frequency-switching (FSw) observing mode at the Yebes-40m radiotelescope, which is currently not being offered to the general public in the open calls.

1   Scientific context and goals

OTF-FSw is a fundamental observing technique that, along with Position Switching (OTF-PSw), allows us to obtain sensitive, homogeneous maps of wide areas in the sky in a very efficient way. While the OTF-PSw technique has been successfully implemented in Yebes-40m, as characterized in Jiménez-Donaire 2020, some settings for the OTF mapping method could be improved, such as the mapping pattern. As seen in Jiménez-Donaire 2020, not turning on the *zigzag* option in the OTF observing scripts resulted in a significant deviation of the mapping coverage. This, in turn, results into an uneven and less sensitive map (Figure 1b).

In order to implement the OTF-FSw observing technique in the Yebes-40m telescope, we will perform a test OTF-FSw map and compare our results to the previous OTF-PSw observations shown in Jiménez-Donaire 2020. One of the best regions to perform such test is the Orion Molecular Cloud Complex, our closest, most extended and best studied star-forming region among all those scattered all over the sky. This system consists of two giant molecular clouds, Orion A and Orion B, being the former the most actively star-forming, hosting the birth of thousands of young stars and protostars. Molecular clouds are fundamental structures of gas and dust which constitute the perfect place where new stars born due to their low temperatures and high densities. Submillimeter and radio observations have revealed the presence of filamentary structures which are rich in molecular gas emission lines (see Bally 2008, Johnstone et al. 1999, Hacar et al. 2020 and references therein for an overview), making this region a great chemical inventory to study. Given its close distance and its brightness, it is an ideal source to test and calibrate new mapping techniques with the Yebes-40m telescope.

By using the same frequency setup used in the testing of the OTF-PSw described in Jiménez-Donaire 2020 we will make use of the uniquely broad W-band window to compare the emission of different density-sensitive molecular gas tracers. In particular, the commonly used dense gas tracers HCN (1-0), HNC (1-0) or HCO^+ (1-0) will be extremely useful to compare the OTF observing capabilities of the Yebes-40m telescope to the recent observations carried at the IRAM-30m (Hacar et al. 2020).

2   Technical justification

We propose to observe the central region of the OMC complex in the OTF-FSw mode, allowing us to characterize this mapping mode at the 40m telescope for the first time. In particular, we suggest observing a part of the 7 pc long integral-shaped filament in the northern side of Orion A. The targeted region is delimited by the black box shown in Figure 1a, and we will observe it as two adjacent maps of 100" x 100", centred in RA 5h 35m 14.16s, DEC +5º 22' 21.5", and RA 5h 35m 14.16s, DEC +5º 20' 42.5", respectively.

Spectral Setup: we will tune the W-band receiver to observe the full frequency range between 86-91 GHz, to obtain similarly comparable spectra to those already obtained while testing the OTF-PSw mode with this telescope (Jiménez-Donaire 2020). We will only need to employ the S7 and S8 chunks, which cover the frequency ranges 86.6 GHz - 89.1 GHz and 88.9 GHz - 91.4 GHz respectively.

Exposure Time: our sensitivity calculations are driven from the previous characterization of the OTF-PSw mode. We do not only aim at detecting the same molecular line species (such as the commonly used dense gas tracers HCN, HNC and HCO^+), but also to achieve a homogeneous, comparable map. Therefore, we will target the same area of interest, consisting on two 100" × 100" maps, and a similar sensitivity as that reached in the PSw mode. Given that our linewidths are typically broad (Figure 2, *left*), a spectral resolution of 38kHz/channel is more than enough to resolve the lines. Typical RMS (in scales of Ta*) values of 0.1K per channel were obtained in the OTF-PSw observations. By using the new online calculator for the OTF-FSw mode, for average summer conditions and an elevation of 45 degrees, we will require a total observing time of ∼2h.

3 Supporting material

(a) Observation region

(b) PSw-OTF Yebes-40m scanning method
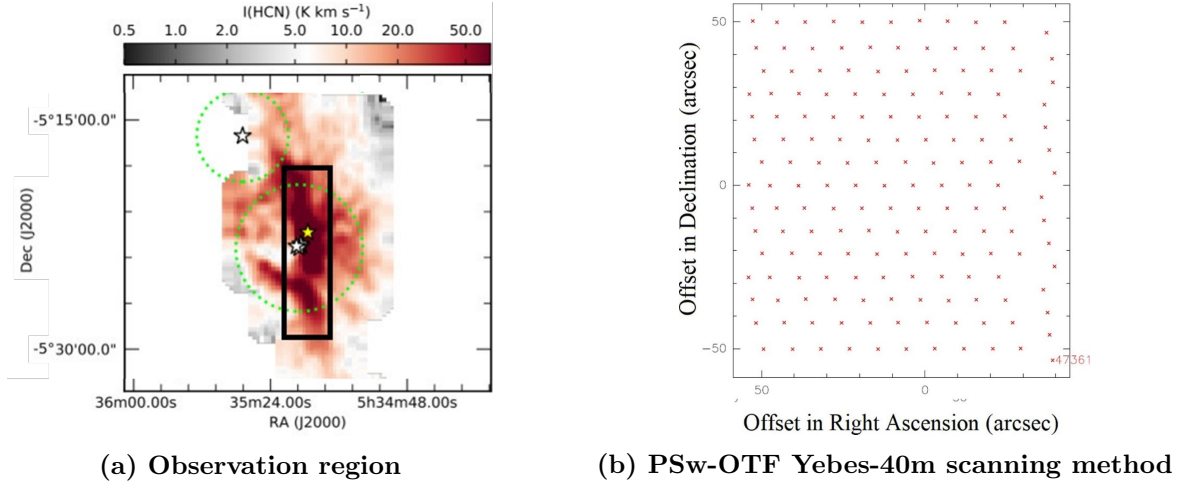
Figure 1. **(a)** Region of interest inside the integral-shaped filament in Orion A (delimited by a black rectangle). This image shows HCN ($J = 1 \rightarrow 0$) distribution in the region, which we will map by splitting it into two 100" x 100 " maps (Figure adapted from Jiménez-Donaire 2020). **(b) PSw-OTF Yebes-40m mapping coverage,** showing a clear deviation towards positive RA offsets in the scanning pattern. The irregular coverage results in lack of sensitivity.
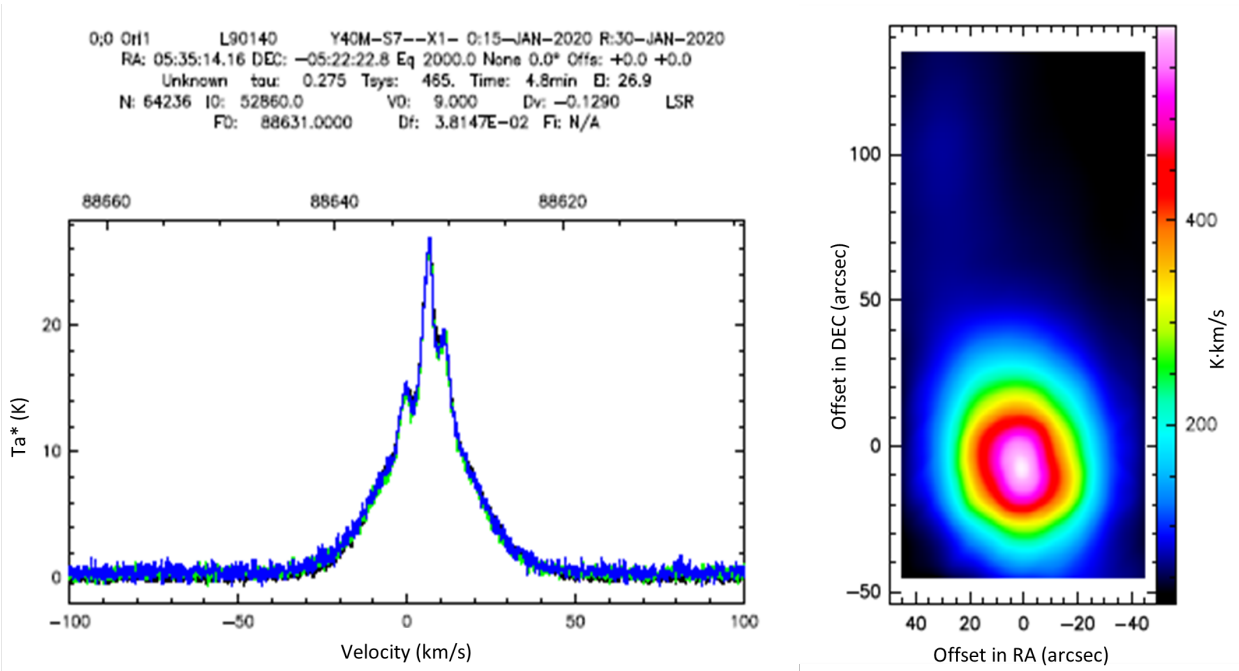
Figure 2. PSw-OTF images with Yebes-40m: Observations made with Yebes-40m telescope. *Left:* central spectrum obtained with Yebes-40m for HCN ($0 \rightarrow 1$). *Right:* HCN ($0 \rightarrow 1$) moment zero map taken with Yebes-40m using the PSw-OTF observing method. The map is centred on RA 5h 35m 14.16s, DEC $+5^{\underline{o}}$ 22' 21.5". Images adapted from Jiménez-Donaire 2020.

References:

Bally, J., 2008, ASP Conference Series ● Johnstone, D. et al. 1999, ApJ, 510, L49 ● Jiménez-Donaire, M. IT-CDT 2020-05 ● Hacar, A. et al. 2018, A&A, 610, A77 ● Hacar, A. et al. 2020, A&A, 635, A4